Self-Acceleration in the Parameterization of Orographic Gravity Wave Drag

JOHN F. SCINOCCA

Canadian Centre for Climate Modelling and Analysis, Environment Canada, Victoria, British Columbia, Canada

BRUCE R. SUTHERLAND

Departments of Physics and of Earth and Atmospheric Sciences, University of Alberta, Edmonton, Alberta, Canada

(Manuscript received 20 October 2009, in final form 26 February 2010)

ABSTRACT

A new effect related to the evaluation of momentum deposition in conventional parameterizations of orographic gravity wave drag (GWD) is considered. The effect takes the form of an adjustment to the basic-state wind about which steady-state wave solutions are constructed. The adjustment is conservative and follows from wave–mean flow theory associated with wave transience at the leading edge of the wave train, which sets up the steady solution assumed in such parameterizations. This has been referred to as ''self-acceleration'' and it is shown to induce a systematic lowering of the elevation of momentum deposition, which depends quadratically on the amplitude of the wave. An expression for the leading-order impact of self-acceleration is derived in terms of a reduction of the critical inverse Froude number F_c, which determines the onset of wave breaking for upwardly propagating waves in orographic GWD schemes. In such schemes F_c is a central tuning parameter and typical values are generally smaller than anticipated from conventional wave theory. Here it is suggested that self-acceleration may provide some of the explanation for why such small values of F_c are required. The impact of F_c on present-day climate is illustrated by simulations of the Canadian Middle Atmosphere Model.

1. Introduction

Orographic gravity wave drag (GWD) parameterizations generally comprise three components: wave sources, conservative wave propagation, and wave dissipation. For the source problem, a steady background flow is assumed in which the undisturbed horizontal background wind U and buoyancy frequency N are constant over the depth of some idealized topographic barrier. The application of steady-state linear theory allows an evaluation of the amount of horizontal momentum that is transported vertically by the wave field. Recent development cycles of orographic GWD schemes have primarily focused on improvements to the wave source component and on the inclusion of low-level drag in the source region (e.g., Lott and Miller 1997; Scinocca and McFarlane 2000, hereafter SM00).

Once the amount of source momentum is determined, the remainder of the parameterization problem is based on a budget for the horizontal momentum (pseudomomentum) of the wave field represented by the wave activity conservation relation:

$$\frac{\partial \mathcal{A}}{\partial t} + \nabla \cdot \mathcal{F} = D, \tag{1}$$

where $\mathcal{A}$ is the pseudomomentum, $\mathcal{F}$ is the pseudomomentum flux, and D represents dissipative sinks of pseudomomentum (e.g., Shepherd 1990). Typically, such schemes assume hydrostatic dynamics and employ steady-state wave solutions for background U and N fields that are assumed to be horizontally uniform and slowly varying in the vertical. These assumptions reduce (1) to

$$\frac{d\mathcal{F}_z}{dz} = D, \tag{2}$$

where $\mathcal{F}_z = \mathcal{F} \cdot \hat{z}$ denotes the vertical transport of horizontal pseudomomentum. For small-amplitude waves, this is just the Reynolds stress $\overline{\rho}\langle uw \rangle$. Ignoring horizontal spatial variations, the exchange of momentum from the wave field to the mean flow is based on the

Corresponding author address: John F. Scinocca, University of Victoria, P. O. Box 3065, STN CSC, Victoria BC V8W 3V6, Canada. E-mail: john.scinocca@ec.gc.ca

DOI: 10.1175/2010JAS3358.1

vertical divergence of the Reynolds stress. This results in steady mean-flow acceleration

$$\frac{\partial U}{\partial t} = -\frac{1}{\bar{\rho}}\frac{\partial \mathcal{F}_z}{\partial z}. \tag{3}$$

Following this approach, we can see from (2) and (3) that all mean flow changes are a direct consequence of dissipative processes (e.g., wave breaking). In the absence of dissipation (i.e., $\partial \mathcal{F}_z/\partial z = 0$), momentum is conserved, and the wave field undergoes conservative propagation in the vertical.

To simplify the modeling of conservative wave propagation and the eventual momentum exchange from the wave field to the background flow, one or two sinusoidal waves are often employed to represent the dynamics of the entire wave field. The onset of wave dissipation is determined by carefully tracking the amplitude of the waves as they propagate vertically through varying U, N, and decreasing ambient density. When the amplitude of the wave field exceeds some prescribed threshold, identified with the onset of instability, it is limited to that threshold, implying a dissipative loss of wave momentum (often referred to as saturation; Lindzen 1981). Following (3), this amount of momentum is transferred from the wave field to the background flow, causing a force that tends to ''drag'' the flow toward the phase speed of the wave.

The procedure described above is based on linear theory, in which the wave field is superimposed on background profiles of U and N supplied by the GCM. It is well known, however, that the transience associated with the presence of the wave field itself alters the background flow (Grimshaw 1975; Dunkerton 1981; Sutherland 2001). This has been referred to as ''self-acceleration'' (Fritts and Dunkerton 1984). As an example, consider the case of a conservatively propagating, vertically localized, wave packet on a constant U and N background flow. This is depicted in the top panel of Fig. 1. As the packet moves upward into regions of undisturbed flow, transience occurs at its leading edge, resulting in $\partial \mathcal{A}/\partial t < 0$ (with $\mathcal{A} < 0$, assuming the wave field carries counterflow momentum associated with a topographic source). For conservative propagation, at the leading edge of the wave packet (1) implies $\nabla \cdot \mathcal{F} > 0$ and so (3) predicts that the amplitude growth results in a force that retards the mean flow. The implication is that the quasi-periodic wave within the packet experiences the adjusted background wind $\widetilde{U}$ rather than U. This mean-flow adjustment is conservative and reversible in the sense that an equal and opposite interaction occurs at the trailing edge of the wave packet. Once the wave packet passes any given point, the background flow is returned to its initial undisturbed value U. Indeed, idealized simulations have shown that for waves of sufficient amplitude, self-acceleration is nonnegligible, causing the extrinsic frequency of the waves themselves to change in response to the self-accelerated flow (Sutherland 2006a).

The interest here arises from the case of an impulsively generated wave train depicted in the bottom panel of Fig. 1. For a vertically propagating wave train, where there exists a continual wave source, transient adjustment occurs at the leading edge of the wave train and the body of the wave train experiences the basic state $\widetilde{U}$, not U, as demonstrated by Sutherland (2006b). This part of the wave train satisfies the wave solution assumed in orographic GWD parameterizations (i.e., steady and sinusoidal), but the implication is that parameterizations should be using $\widetilde{U}$ and not U in their calculations for conservative propagation and dissipative wave–mean flow interaction. In this study we consider the impact of self-acceleration on an existing parameterization of orographic GWD (SM00).

The outline of the paper is as follows. In section 2 we derive an expression for $\widetilde{U}$ suitable for application in orographic GWD schemes and discuss its implementation in the SM00 GWD parameterization. In section 3 we investigate the impact of self-acceleration in the SM00 scheme by performing present-day climate simulations of the Canadian Middle Atmosphere Model (CMAM). Finally, in section 4 we conclude with a brief summary and discussion regarding the implications of these results.

2. Self-acceleration

a. Wave-induced mean flow

Following Scinocca and Shepherd (1992) and Sutherland (2006b), the leading-order wave-induced mean flow associated with transience at the leading edge of a sinusoidal wave packet is

$$U' = -\langle \xi\zeta \rangle, \tag{4}$$

in which ξ is the vertical displacement and $\zeta = \partial_z u - \partial_x w$ is the vorticity due to waves; the angle brackets denote horizontal averaging. This relation holds both for a Boussinesq fluid as well as for an anelastic gas. Using the polarization relations for internal waves in an anelastic gas, we can write the amplitude A_ζ of ζ in terms of the amplitude of the vertical displacement field. Explicitly,

$$\left|A_\zeta\right| = \frac{N^2}{|U|}|A|. \tag{5}$$

Here, we have assumed that the orographically generated waves are stationary so that their wind-relative

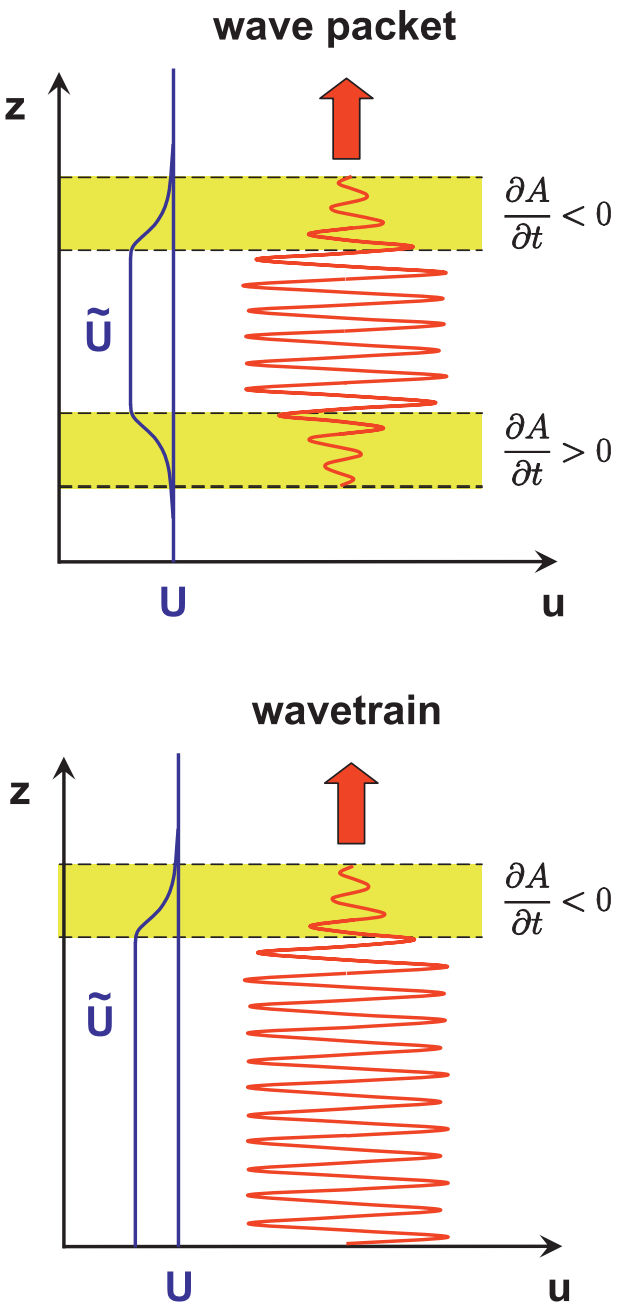

FIG. 1. (top) Vertically propagating gravity wave packet in a constant U and N background. As the packet moves upward into the undisturbed flow wave transience occurs ($\partial\mathcal{A}/\partial t < 0$) at its leading edge (with $\mathcal{A} < 0$, assuming the wave field carries counterflow momentum associated with a topographic source). From (1) and (3) this implies a force on the mean flow, which causes a deceleration of the wind to $\tilde{U}$ within the wave packet. This is referred to as self-acceleration. Because this is a conservative force, as the trailing edge moves through the fluid an equal and opposite interaction occurs and the flow returns to its undisturbed conditions after the passage of the wave packet. (bottom) As at top, but for an impulsively generated wave train. In this instance the same wave–mean flow interaction takes place at the leading edge of the wave field. However, since there is a continual source of waves the

frequency has magnitude $|Uk|$. Together with (4), we have

$$|U'| = \frac{1}{2}\frac{N^2}{|U|}A^2. \tag{6}$$

Employing the natural length scale U/N to nondimensionalize the amplitude at each height, the total flow seen by the interior of the packet, which includes the self-accelerated flow, is written

$$\tilde{U} = U + U' = U\left(1 - \frac{F^2}{2}\right), \tag{7}$$

where

$$F = NA/U \tag{8}$$

is the nondimensional amplitude of the wave, often referred to as the inverse Froude number. The sign of U' is such that the transience at the leading edge of the packet drags the mean wind toward its phase speed of zero. This in turn affects the structure of the waves. Evident in the form of the nonlinear Schrödinger equation given by Sutherland (2006b), the effective change in wind speed Doppler shifts the wave frequency. In particular, this means that the vertical wavenumber of hydrostatic orographic waves shifts in magnitude from $N/|U|$ to $N/|\tilde{U}|$.

Note that conservation of mass means that the horizontally averaged density is not altered at second order in wave amplitude: internal waves transport momentum, not mass. The effect of the decrease with height of background density $\overline{\rho}$ is implicitly included in (6) through the increase with height of the vertical displacement A so that $\overline{\rho}U'$ is constant as the waves propagate upward. Likewise, conservation of internal energy means that the horizontally averaged potential temperature is not altered at second order. Hence, the overturning condition, given in terms of gradients of the potential temperature $\partial(\overline{\theta} + \theta')/\partial z < 0$, is well represented at leading order by gradients of the vertical displacement field: $\partial\xi/\partial z > 1$, in which the fluctuation potential temperature is given in terms of the vertical displacement at leading order by $\theta' = -\xi d\overline{\theta}/dz$.

←

adjustment is not reversed and the entire wave train sees the background wind $\tilde{U}$. Here, the wave train is associated with the wave field modeled by orographic GWD parameterization schemes.

b. Application to orographic GWD

An obvious way to include the self-acceleration effect (7) in an orographic GWD parameterization is to employ $\widetilde{U}$ rather than U in all calculations of wave propagation and dissipation. It is useful to review the procedure by which conservative propagation and dissipation of a sinusoidal wave is typically modeled in orographic GWD schemes to identify how best to implement this change.

Profiles of background U and N, supplied by the large-scale GCM to the parameterization at each time step, are assumed to be steady and slowly varying in the vertical. As a wave propagates vertically, its amplitude changes because of the vertical variations of $U(z)$ and $N(z)$ and the exponential decrease of ambient density with height. Dissipation of the wave is determined by comparing a nondimensional measure of its amplitude on each successive model level. Explicitly, this is done by comparing the local F against some threshold value F_c marking the onset of wave instability and breaking. When $F \leq F_c$ no dissipation occurs and the wave is considered to be conservatively propagating to the next model level. When $F > F_c$, dissipation is thought to occur and the amplitude of the wave is explicitly reduced to $F = F_c$ before being allowed to propagate up to the next level. The reduction of the wave amplitude implies a loss of momentum from the wave and this is the amount of momentum transferred to the basic state on that level. This treatment is referred to as saturation; the detailed implementation used in this study may be found in McFarlane (1987).

Using $\widetilde{U}$ in place of U in the above procedure means that the inverse Froude number (10) is appropriately redefined as

$$\widetilde{F} = NA/\widetilde{U} = \frac{F}{(1 - F^2/2)}, \tag{9}$$

where the final expression follows from (7). The criterion for the onset of dissipation then changes from $F = F_c$ to

$$\widetilde{F} = F_c = \frac{F}{(1 - F^2/2)}, \tag{10}$$

following (9). Solving (10) for F defines a new "effective" critical amplitude $\widetilde{F}_c$. Therefore, at leading order, modifying an orographic GWD scheme to use $\widetilde{U}$ in place of U is equivalent to using $\widetilde{F}_c$ in place of F_c in the unmodified scheme.

The functional relationship of $\widetilde{F}_c$ relative to F_c is obtained by solving (10) for F. This is illustrated in Fig. 2 (solid line) indicating that $\widetilde{F}_c$ is always smaller than F_c.

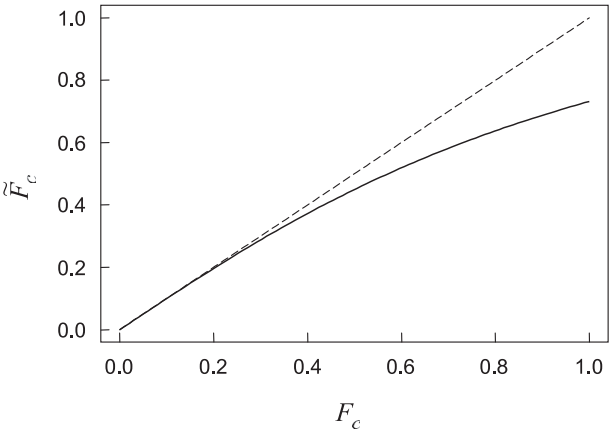

FIG. 2. Plot of $\widetilde{F}_c$ as a function of F_c (solid line) derived from (10). The use of $\widetilde{F}_c$ in place of the input value of F_c in the orographic GWD scheme accounts for the leading-order impact of self-acceleration.

This implies that the effect of self-acceleration is to cause waves to break at smaller amplitude and, therefore, to break systematically at lower elevation relative to the default scheme.

The wave overturning value (F_c) entering into (10) depends on a number of factors. In the absence of all nonlinearity and wave transience, the linear theory condition for overturning of hydrostatic internal waves is $F_c = 1$. However, for a stationary wave solution over a localized obstacle, it is well known that overturning depends on nonlinearity associated with the height, shape, and hydrostatic nature of the obstacle (e.g., Laprise and Peltier 1989). For the well-studied "witch of Agnesi" two-dimensional ridge, Miles and Huppert (1969) were the first to show that such nonlinearity resulted in overturning at the significantly reduced value of $F_c = 0.85$ for stationary hydrostatic waves. Upstream/downstream asymmetry of the topographic profile can have an even greater impact on the value of F_c. For example, Miller and Durran (1991) considered the witch of Agnesi ridge with varying upstream versus downstream half widths. For half-width ratios (upstream:downstream) ranging from 10:1 to 1:10, they found that F_c ranged in value from 0.56 to 1.00 (their Table 1). For any of these values of F_c, the analysis presented here would suggest that each could be reduced to their corresponding $\widetilde{F}_c$ following Fig. 2.

In practice, orographic GWD schemes employ a single representative value of F_c. Typical values include $F_c = (0.5)^{1/2} \simeq 0.71$ in the McFarlane (1987) and SM00 schemes used in the Canadian Centre for Climate Modeling and Analysis (CCCma) third-generation tropospheric general circulation model (Scinocca et al. 2008) and $F_c = 0.5$ in the Webster et al. (2003) scheme employed by the Hadley Centre Global Environmental

Model, which is reduced to $F_c = 0.25$ for numerical weather prediction applications. More recently, a value $F_c = 0.375$ has been employed in the SM00 scheme for the Canadian Middle Atmosphere Model to improve lower stratospheric polar temperatures for chemistry–climate simulations (Scinocca et al. 2008). While any of these values of F_c could be argued as arising from nonlinearity associated with a particular lower boundary forcing, they would seem too small to be argued as representative values for the spectrum of topographic obstacles parameterized by orographic GWD in a GCM.

In this regard, the systematic reduction of F_c implied by the effect of self-acceleration provides some argument for the use of lower representative values of F_c in current orographic GWD schemes. At the same time, however, it is important to note that the reduction of F_c to $\widetilde{F}_c$ illustrated in Fig. 2 becomes progressively smaller as F_c is lowered. Consequently, self-acceleration can only provide some of the explanation for the use of such small representative values of F_c. In the next section we will consider the impact of self-acceleration by varying the value of F_c in the SM00 scheme in simulations of present-day climate.

3. Present-day climate experiments

In this section we employ the CMAM (Scinocca et al. 2008) to illustrate the impact of including the self-acceleration effect in the parameterization of orographic gravity wave drag. CMAM is an upward-extended version of the CCCma third-generation tropospheric general circulation model (AGCM3) (Scinocca et al. 2008). Both AGCM3 and CMAM employ the SM00 parameterization of orographic gravity wave drag with default values of $F_c \simeq 0.71$ in AGCM3 and 0.375 in CMAM (see section 3.3 of Scinocca et al. 2008). The results presented in this section are based on climatologies derived from 5-yr simulations of the CMAM employing a spectral resolution with triangular truncation at total wavenumber 47. In the vertical the model employs 71 levels from the surface to roughly 100-km elevation (see Scinocca et al. 2008). The leading-order impact of self-acceleration is illustrated by adjusting F_c in the SM00 scheme from its AGCM3 typical value (0.71).

In Fig. 3 the climatological zonal mean zonal wind is presented for (left) Northern Hemisphere (NH) winter [December–February (DJF)] and (right) Southern Hemisphere (SH) winter [June–August (JJA)]. The observed climate (Randel et al. 2004) is presented in the first row (Figs. 3a,b). The remaining three rows of Fig. 3 present the climatological winds from three CMAM simulations. The first row (Figs. 3c,d) corresponds to a simulation of CMAM using the default AGCM3 value of F_c. A comparison of the winds in the CMAM control with those in the observations reveals several biases. The particular bias of interest occurs in the wintertime polar lower stratosphere. This is clearest in the NH where it is seen that CMAM's winds are weaker in the neck region between the tropospheric and stratospheric jets near 45°–80°N and 100–50 hPa (cf. Figs. 3a and 3c).

In Figs. 4a and 4b the observed zonal mean zonal temperature fields are presented. The remaining panels of Fig. 4 present temperature anomaly plots away from these observations for each of the three CMAM simulations presented in Fig. 3. Inspection of Figs. 4c and 4d reveals that the weak winds in the wintertime polar lower stratosphere are associated with a warm bias near 50 hPa at the wintertime poles. This is now apparent in both the NH (Fig. 4c) and SH (Fig. 4d). While there are a number of wind and temperature biases elsewhere, these biases have important consequences for stratospheric ozone evolution and high-latitude climate change. The high-latitude temperatures are connected to the winds through thermal wind balance (e.g., Andrews et al. 1987), which connects the vertical gradient of wind to the meridional gradient of temperature.

The impact of reducing F_c from $F_c \simeq 0.71$ to $F_c \simeq 0.586$ is displayed in the third row of Figs. 3 and 4. The value $F_c \simeq 0.586$ corresponds to the $\widetilde{F}_c$ derived from Fig. 2 using $F_c \simeq 0.71$. This reduction is equivalent to applying the effects of self-acceleration to the default settings of the SM00 scheme used in AGCM3. From Figs. 4e and 4f it can be seen that this change in F_c causes a modest 1 K reduction of warm bias in the lower stratosphere (near 50 hPa) at the wintertime poles. This change is less apparent in the wind field.

The impact of reducing F_c is clearer when its value is reduced even further. In the final row of Figs. 3 and 4 the wind and temperature climatology for $F_c = 0.375$ is displayed. As discussed earlier, $F_c = 0.375$ corresponds to the default settings employed by CMAM. From Fig. 3 it can be seen that this reduction in F_c increases the wind in the neck region in the lower stratosphere of the wintertime poles (see Fig. 3g in particular). This produces a stronger vertical wind gradient in the region from 50° to 90°N near 50 hPa (Fig. 3g) and, through thermal wind balance, colder polar temperatures as seen in Fig. 4g. The temperature bias is reduced by nearly 8° in DJF at the North Pole. For this value of F_c it can be seen that the JJA warm bias at the South Pole near 50 hPa has been reversed from a 7° warming to roughly a 1° cooling. Aloft, the JJA Southern Hemisphere jet near 2 hPa (Figs. 3h and 4h) is too strong and too cold relative to observations. At these elevations nonorographic GWD plays an important role and such biases may be less relevant to orographic GWD.

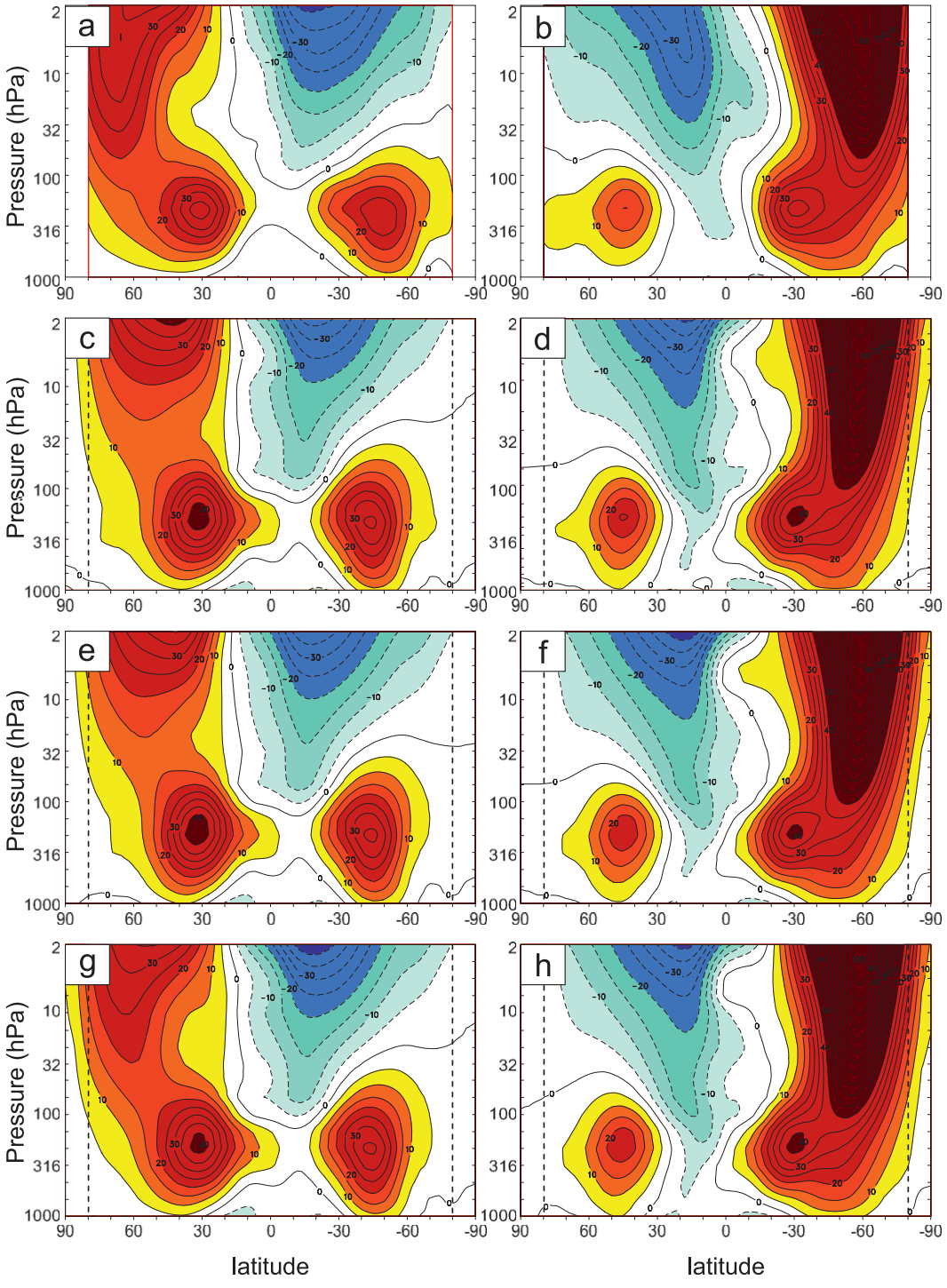

FIG. 3. Climatological zonal-mean zonal wind for (left) NH winter (DJF) and SH winter (JJA). (a),(b) The observed climate (Randel et al. 2004). (c)–(h) Results from three runs of CMAM employing (c),(d) the default value of $F_c \sim 0.71$, (e),(f) the corresponding value $F_c \sim 0.586$ derived from Figs. 2e,f, and (g),(h) $F_c \sim 0.372$.

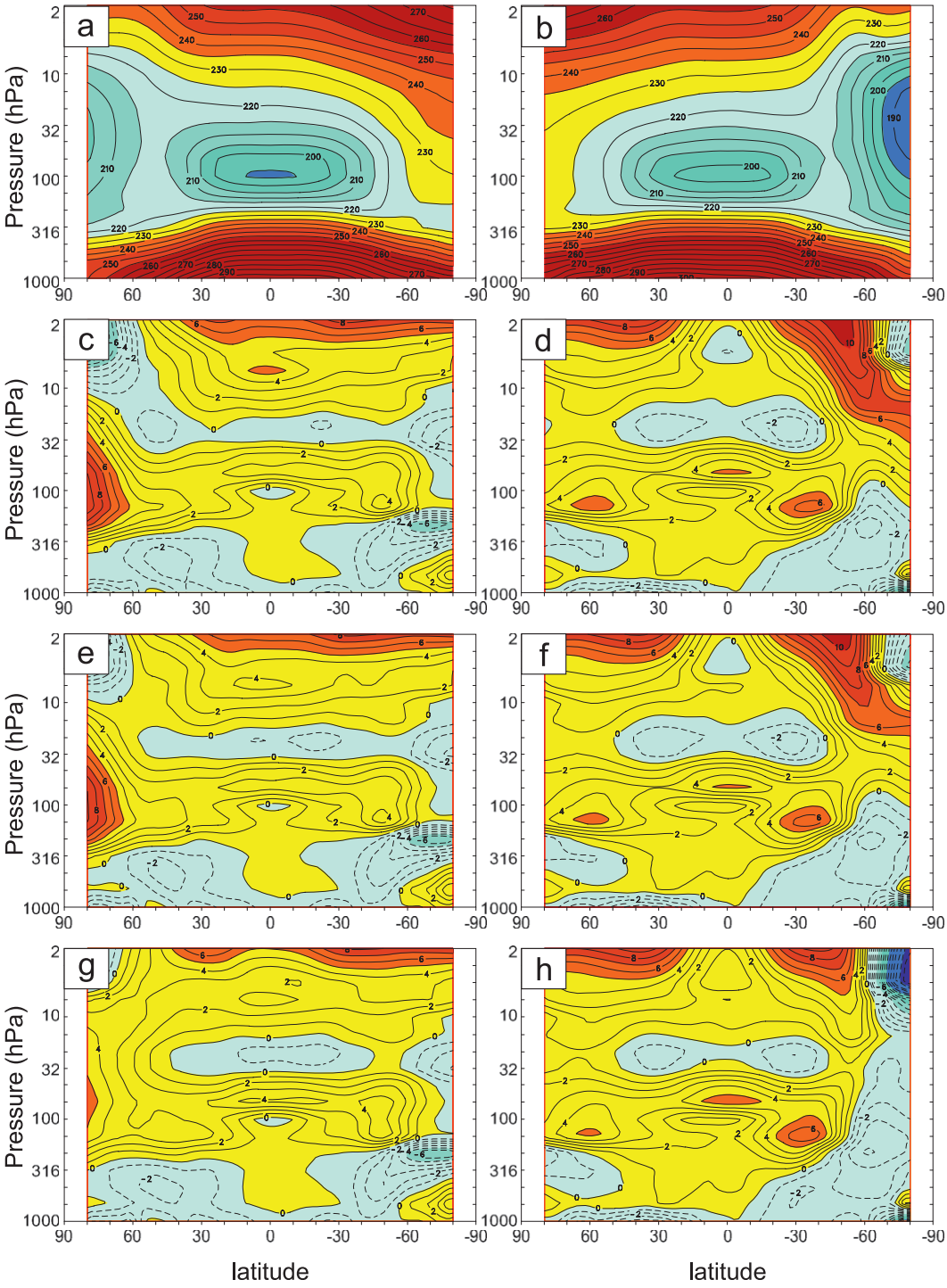

FIG. 4. As in Fig. 3, but for (a),(b) the observed zonal-mean temperature (K) and (c)–(h) the temperature biases relative to these observations. The impact of reducing F_c below its default value targets mainly the lower stratosphere of the wintertime poles near 50 hPa. The biases here relative to observations are seen to improve with decreasing F_c.

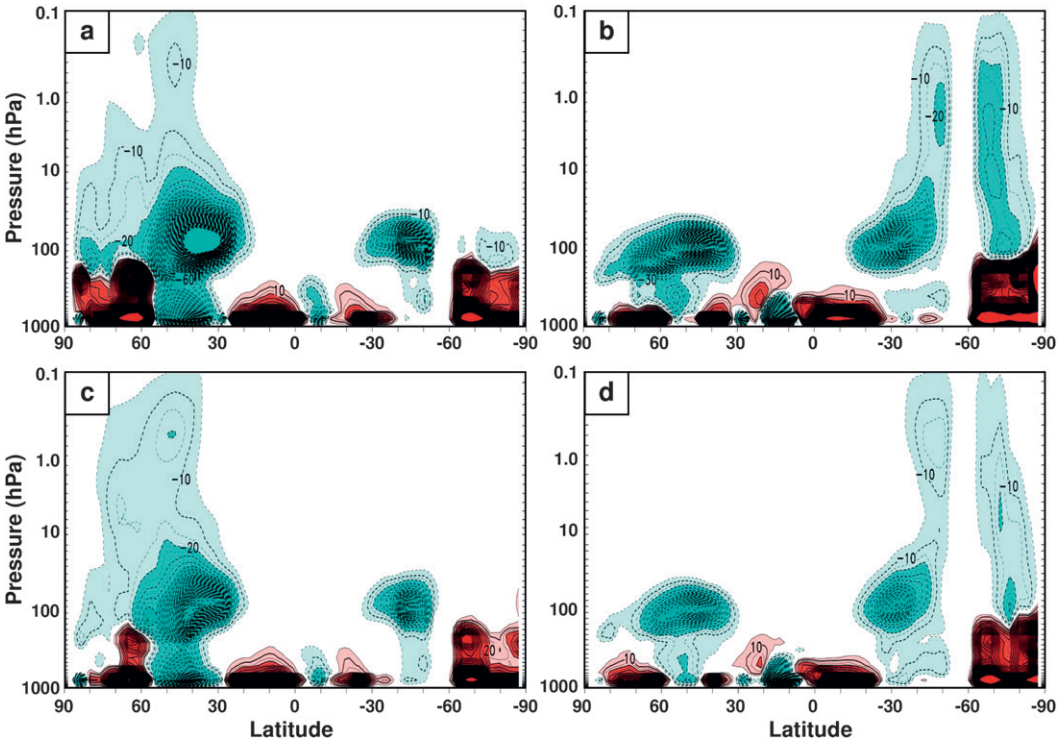

FIG. 5. Climatological zonal-mean orographic GWD (Pa m^{-1}) for (left) NH winter (January) and (right) SH winter (July), corresponding to (a),(b) the run of CMAM employing $F_c \sim 0.71$ and (c),(d) $F_c \sim 0.372$. Orographic GWD in the stratosphere is most prominent at high latitudes in winter and the reduction of F_c results in a general reduction of drag in this region consistent with the wind response in Fig. 3.

The overall impact of reducing F_c from its AGCM3 default value of 0.71 in CMAM is beneficial in that it reduces wintertime polar wind and temperature biases in the lower stratosphere. It can be seen from Figs. 3 and 4 that the changed F_c targets these regions and periods almost exclusively. That is, wind and temperature biases are essentially left unaffected elsewhere and during other periods.

In Fig. 5 the climatological zonal mean orographic GWD is presented for (left) Northern Hemisphere winter (January) and (right) Southern Hemisphere winter (July) for the two values of $F_c = 0.71$ (Figs. 5a,b) and $F_c = 0.375$ (Figs. 5c,d). It can be seen that orographic GWD in the stratosphere is located predominantly at high latitudes in the winter hemisphere. The reduction of F_c generally results in a reduction of orographic GWD in these regions, consistent with the wind response in Fig. 3.

4. Summary

Currently, the criteria for wave steepening and overturning in the parameterization of orographic GWD are based conceptually on a combination of linear wave theory and nonlinearities associated with properties of the underlying orography. Here we have extended this conceptual basis to include nonlinear effects associated with large-amplitude propagating waves, referred to as self-acceleration. In this paper we have considered the way in which self-acceleration alters the formulation of momentum deposition in the parameterizations of orographic gravity wave drag. Self-acceleration is associated with a conservative, wave-induced, mean-flow adjustment of the horizontal wind, which depends quadratically on the amplitude of the wave. For an impulsively generated vertically propagating wave train, the magnitude of the mean horizontal wind seen by the body of the wave field is reduced. The leading-order effect is an increase in the amplitude of the wave train when self-acceleration is included. Larger wave amplitudes imply that vertically propagating waves systematically break at lower elevations.

We have expressed the leading-order effect of self-acceleration in a way that may be easily related to parameterizations of orographic gravity wave drag. The systematic increase in wave amplitude effectively implies a systematic reduction in the critical inverse Froude number F_c, which is the nondimensional wave amplitude threshold employed to determine the onset of wave

dissipation. An expression for the effective critical inverse Froude number $\widetilde{F}_c$, which takes the leading-order effect of self-acceleration into account, is given by (10) and is displayed in Fig. 2. The prescription to include the effects of self-acceleration in any parameterization of orographic gravity wave would be the use of $\widetilde{F}_c$ in place of F_c when determining wave dissipation.

As discussed in this paper, nonlinearity of the lower boundary forcing can result in specific values of F_c that extend over an enormous range (e.g., 0.5–1.0). Orographic parameterization schemes use one representative value of F_c for all circumstances. Current operational schemes use values for F_c that are too low to be argued as representative of all circumstances. For example, the SM00 scheme employed by CCCma uses values that range from 0.71 to 0.375 while the Webster et al. (2003) scheme employed by the Hadley Centre uses values that range from 0.5 to 0.25. Given that F_c is a tunable parameter in orographic GWD schemes, one could assume that the impact of self-acceleration is already included in the optimized value of F_c used by a model, which may depend on a variety of model-dependent factors. Here we have argued that self-acceleration provides some explanation for the use of such small F_c values in current orographic parameterization schemes.

The impact of including self-acceleration in the SM00 parameterization of orographic gravity wave drag has been illustrated in present-day climate simulations of the Canadian Middle Atmosphere Model (CMAM). Multiyear present-day climate runs of CMAM were performed with the AGCM3 default value of $F_c = 0.71$ and a reduced value of 0.586 determined from (10). Applying self-acceleration to the AGCM3 default value resulted in a small but detectable reduction in wind and temperature biases at both wintertime poles in the lower stratosphere. The model winds in CMAM are typically too weak and the climate too warm in these locations in wintertime; the inclusion of self-acceleration causes an increase in the wind speed and, through thermal wind balance, a cooling of the pole.

The robustness of the improvement realized by reducing F_c from 0.71 to 0.586 is evidenced by the more dramatic but similarly structured response obtained when F_c is further reduced to the CMAM default value of 0.375. This last experiment highlighted the fact that changes to F_c seem to preferentially target the winds and temperatures of the wintertime polar lower stratosphere. The present-day climate associated with the CMAM default value of F_c showed a more significant reduction of wind and temperature biases. It is clear that self-acceleration cannot on its own fully justify the use of such small F_c in current applications of orographic GWD schemes. Self-acceleration does, however, imply a systematic reduction of the value of F_c derived from conventional internal wave theory and in this sense may provide some of the explanation.

Finally, there is evidence that wintertime polar wind biases associated with the specific value of F_c can have a significant influence on the dynamical response to climate change in the Northern Hemisphere. Modeling extratropical climate change in NH winter is a challenge (e.g., Solomon et al. 2007) as there currently exists a wide range in the projected response in that region—particularly that part of the response that projects onto the northern annular mode (NAM; Thompson and Wallace 2000; Miller et al. 2006). In a recent study by Sigmond and Scinocca (2009), CO_2 doubling experiments were performed to investigate the properties of the NAM response under climate change. It was found that the NAM response was very sensitive to lower-stratospheric wintertime wind biases of the initial control climate upon which the CO_2 perturbation was applied. One of the main conclusions of the Sigmond and Scinocca (2009) study was that the NAM response to climate change should be expected to be sensitive to any physical process that alters the winds of the control climate in this region (e.g., solar variability and settings of the orographic GWD parameterization). The fact that the self-acceleration in the parameterization of orographic GWD accounts for some of the reduction in wind biases in this critical region means that it has some responsibility for improving the credibility of future projections of climate change.

Acknowledgments. The authors thank Norm McFarlane for gratefully carefully reading the manuscript and providing helpful suggestions. This research has been supported by the Canadian Foundation for Climate and Atmospheric Sciences.

REFERENCES

Andrews, D. G., J. R. Holton, and C. B. Leovy, 1987: *Middle Atmosphere Dynamics*. Academic Press, 489 pp.

Dunkerton, T. J., 1981: Wave transience in a compressible atmosphere. Part I: Transient internal wave, mean-flow interaction. *J. Atmos. Sci.,* **38,** 281–297.

Fritts, D. C., and T. J. Dunkerton, 1984: A quasi-linear study of gravity-wave saturation and self-acceleration. *J. Atmos. Sci.,* **41,** 3272–3289.

Grimshaw, R., 1975: Nonlinear internal gravity waves and their interaction with the mean wind. *J. Atmos. Sci.,* **32,** 1779–1793.

Laprise, R. J., and W. R. Peltier, 1989: On the structural chracteristics of steady finite-amplitude mountain waves over bell-shaped topography. *J. Atmos. Sci.,* **46,** 586–595.

Lindzen, R. S., 1981: Turbulence and stress owing to gravity wave and tidal breakdown. *J. Geophys. Res.,* **86,** 9707–9714.

Lott, F., and M. Miller, 1997: A new subgrid-scale orographic drag parameterization: Its formulation and testing. *Quart. J. Roy. Meteor. Soc.,* **123,** 101–127.

McFarlane, N. A., 1987: The effect of orographically excited gravity wave drag on the general circulation of the lower stratosphere and troposphere. *J. Atmos. Sci.,* **44,** 1775–1800.

Miles, J. W., and H. E. Huppert, 1969: Lee waves in a stratified flow. Part 4. Perturbation approximations. *J. Fluid Mech.,* **35,** 497–525.

Miller, P. P., and D. R. Durran, 1991: On the sensitivity of downslope windstorms to the asymmetry of the mountain profile. *J. Atmos. Sci.,* **48,** 1457–1473.

Miller, R. L., G. A. Schmidt, and D. T. Shindell, 2006: Forced annular variations in the 20th century Intergovernmental Panel on Climate Change Fourth Assessment Report models. *J. Geophys. Res.,* **111,** D18101, doi:10.1029/2005JD006323.

Randel, W. J., and Coauthors, 2004: The SPARC intercomparison of middle-atmosphere climatologies. *J. Climate,* **17,** 986–1003.

Scinocca, J. F., and T. G. Shepherd, 1992: Nonlinear wave-activity conservation laws and Hamiltonian structure for the two-dimensional anelastic equations. *J. Atmos. Sci.,* **49,** 5–28.

——, and N. A. McFarlane, 2000: The parameterization of drag induced by stratified flow over anisotropic orography. *Quart. J. Roy. Meteor. Soc.,* **126,** 2353–2393.

——, ——, M. Lazare, J. Li, and D. Plummer, 2008: The CCCma third generation AGCM and its extension into the middle atmosphere. *Atmos. Chem. Phys.,* **8,** 7055–7074.

Shepherd, T. G., 1990: Symmetries, conservation laws, and Hamiltonian structure in geophysical fluid dynamics. *Adv. Geophys.,* **32,** 287–338.

Sigmond, M., and J. F. Scinocca, 2009: The influence of basic state on the Northern Hemisphere circulation response to climate change. *J. Climate,* **23,** 1434–1446.

Solomon, S., D. Qin, M. Manning, Z. Chen, M. Marquis, K. B. Averyt, M. Tignor, and H. L. Miller, Eds., 2007: *Climate Change 2007: The Physical Science Basis*. Cambridge University Press, 996 pp.

Sutherland, B. R., 2001: Finite-amplitude internal wavepacket dispersion and breaking. *J. Fluid Mech.,* **429,** 343–380.

——, 2006a: Internal wave instability: Wave–wave vs wave-induced mean flow interactions. *Phys. Fluids,* **18,** 074107, doi:10.1063/1.2219102.

——, 2006b: Weakly nonlinear internal gravity wavepackets. *J. Fluid Mech.,* **569,** 249–258.

Thompson, D. W. J., and J. M. Wallace, 2000: Annular modes in the extratropical circulation. Part I: Month-to-month variability. *J. Climate,* **13,** 1000–1016.

Webster, S., A. R. Brown, D. R. Cameron, and C. P. Jones, 2003: Improvements to the representation of orography in the Met Office Unified Model. *Quart. J. Roy. Meteor. Soc.,* **129,** 1989–2010.